Science Advances
AAAS

Supplementary Materials for

In vivo mapping of cellular resolution neuropathology in brain ischemia with diffusion MRI

Dan Wu *et al.*

Corresponding author: Dan Wu, danwu.bme@zju.edu.cn; Jiangyang Zhang, jiangyang.zhang@nyulangone.org

Sci. Adv. **10**, eadk1817 (2024)
DOI: 10.1126/sciadv.adk1817

This PDF file includes:

Figs. S1 to S9
Tables S1 to S8

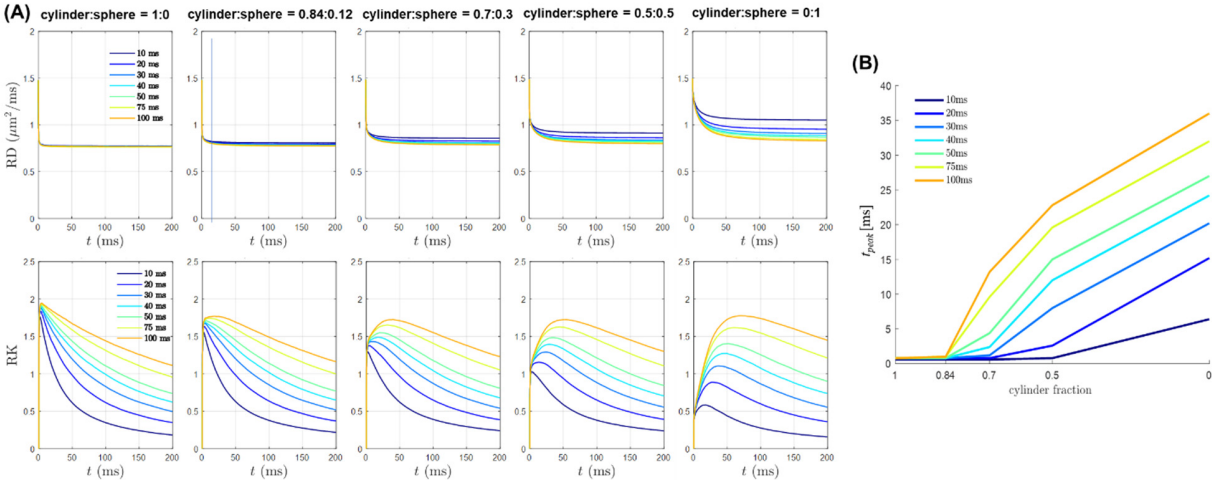

Fig. S1. Monte-Carlo simulations of the mixed phantom of cylinders and spheres. The cylinders were set at 1.2 μm diameter with a dispersion degree of 40º, and spheres were set at 12 μm. The cylinders and spheres were combined at the signal level with different ratios, both at an intracellular volume fraction of 50%. **(A)** The *t*-dependent changes in diffusivity and kurtosis with varying transmembrane exchange times (τ_{ex}, from 10-100ms). **(B)** The change in peak time (t_{peak}) with the fraction of cylinders (from 1 to 0) and τ_{ex} (from 10-100ms).

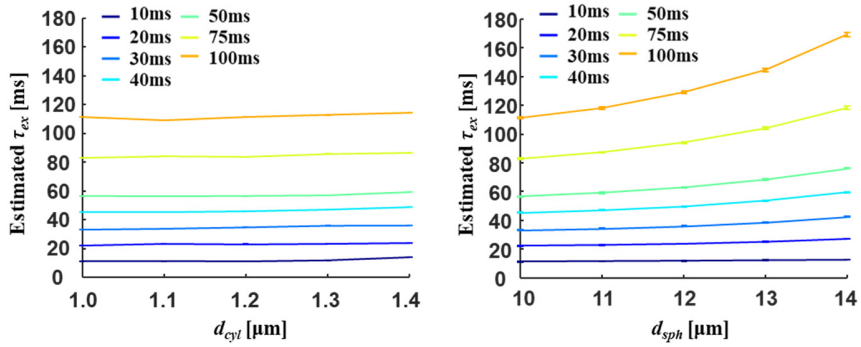

Fig. S2. The relationship between the estimated τ_{ex} and the sizes of cylinders and spheres in the simulations. The change in the estimated τ_{ex} with the cylinder size ranging from 1.0 to 1.4 µm and the preset τ_{ex} ranging from 10 to 100 ms, while the sphere size was fixed at 10 µm (left); and the change in τ_{ex} with the sphere size ranging from 10 to 14 µm and the preset τ_{ex} ranging from 10 to 100 ms, while the cylinder size was fixed at 1.0 µm (right). Note the estimated τ_{ex} deviated from the preset values for large spheres, potentially because the diffusion inside large spheres was still not approximately Gaussian at the t scale used in simulations (i.e., t is not long enough for large spheres) and thus did not meet the Gaussian assumption of the Kärger model in these scenarios.

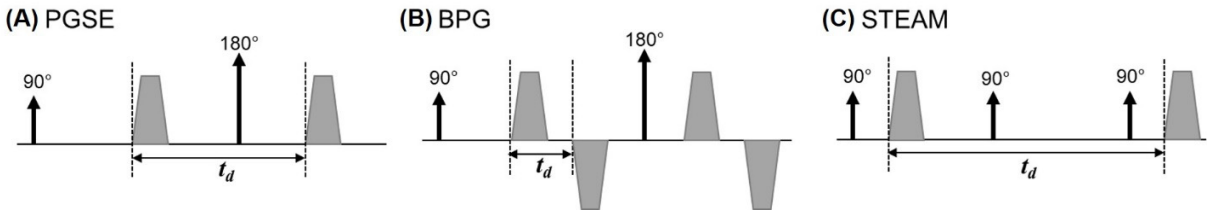

Fig. S3. Schematics of the pulse sequences for different diffusion encoding schemes. (A) pulsed gradient spin-echo (PGSE), **(B)** bipolar pulsed gradient (BGP), and **(C)** stimulated echo acquisition mode (STEAM). The effective diffusion time (t_d) are indicated in each scheme.

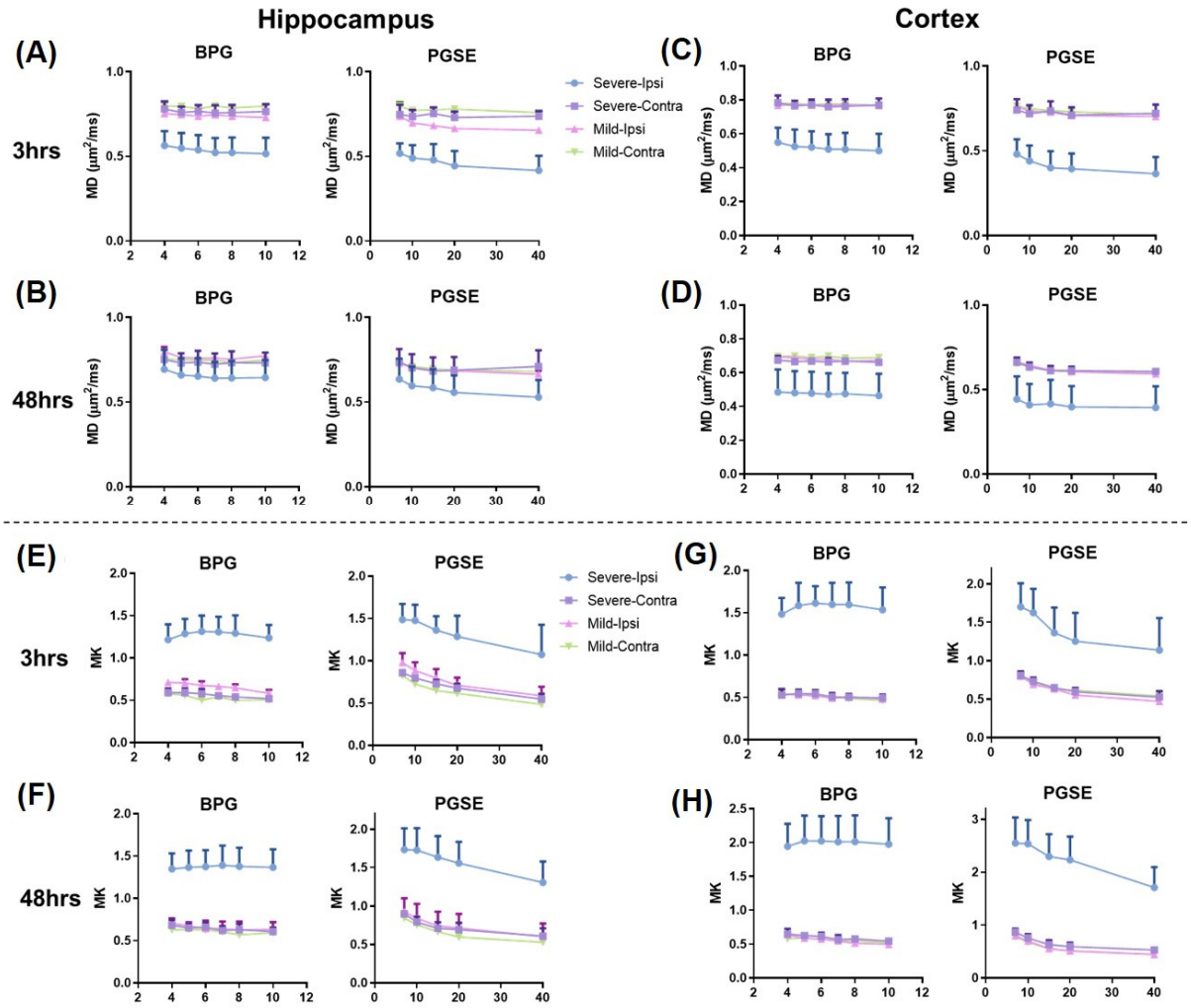

Fig. S4. *t*-dependent change in mean diffusivity (MD) and mean kurtosis (MK). **(A-D)** MD, and **(E-H)** MK measured in the hippocampus and cortex of HI-injured mouse brains at 3 hrs and 48 hrs after injury, using the BGP and PGSE sequences.

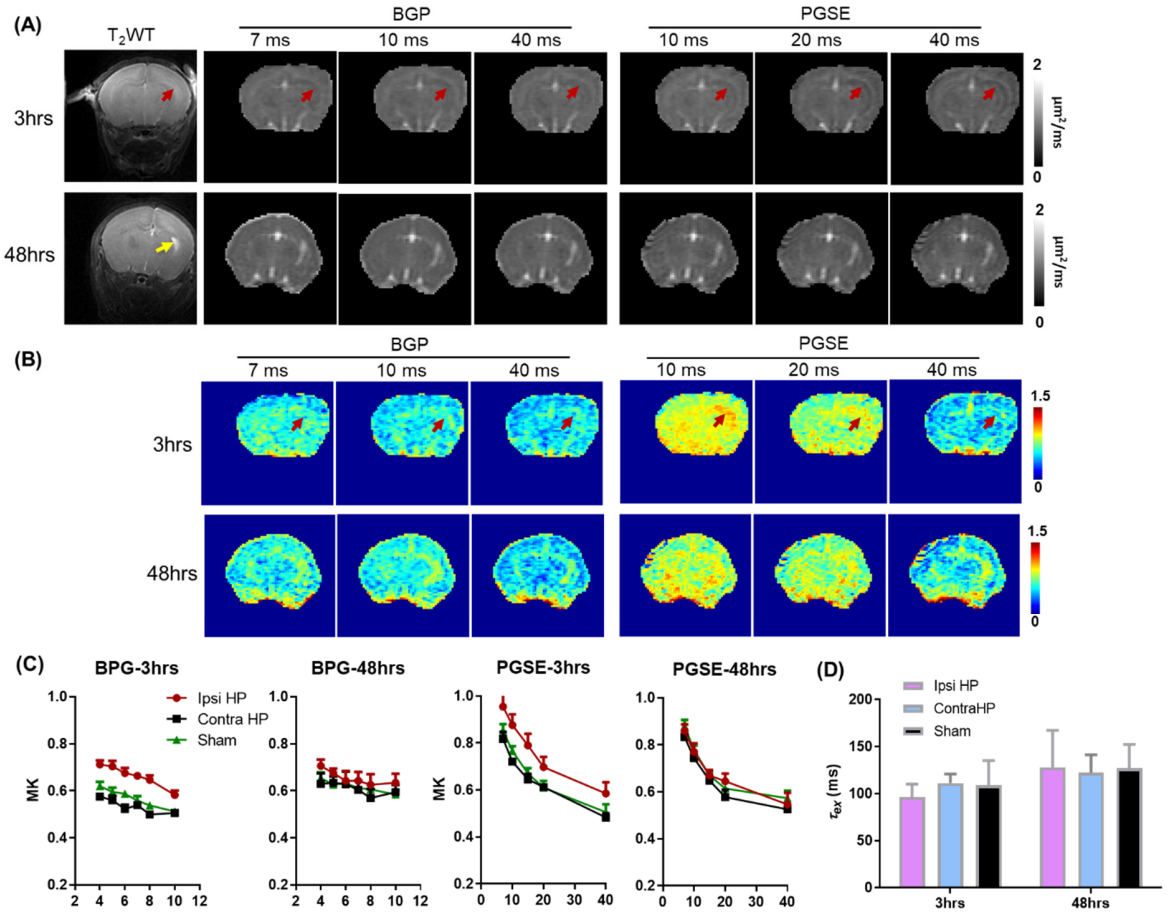

Fig. S5. *t*DKI in HI-injured mice with mild-to-moderate injury. (A-B) Diffusivity and kurtosis maps of a moderately injured mouse brain scanned at 3 hrs and 48 hrs after the HI onset with *t* ranging from 4-40 ms, using a combination of BPG and PGSE sequences. The red arrows point to reduced diffusivity and elevated kurtosis in the ipsilateral hippocampus at 3 hrs, which eventually led to cell death and enlarged ventricle at 48 hrs (yellow arrow). **(C)** *t*-dependent change in mean kurtosis (MK) between 4-10 ms did not show an apparent kurtosis peak, and kurtosis tails showed a similar rate of decay between 7-40 ms. **(D)** Statistical comparison of τ_{ex} between the ipsilateral and contralateral hippocampus and sham mice did not show statistical difference, either at 3 hrs (n=10) or 48 hrs (n=5) after HI.

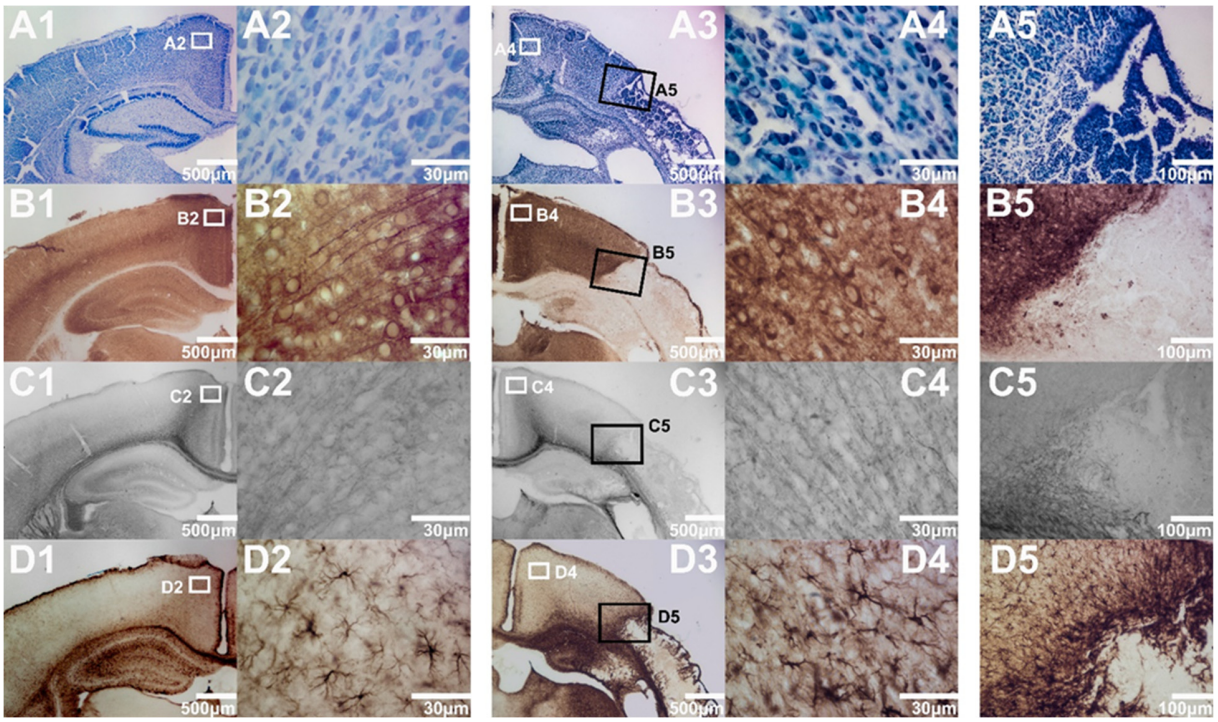

Fig. S6. Pathology of the neurons, astrocytes, and cellular processes of a neonatal brain at 48 hrs after HI injury, corresponding to the mouse brain in Fig. 5. (A) Nissl staining of the contralateral **(A1)** and ipsilateral **(A3)** brain with zoomed-in views of the cingulate cortex **(A2** and **A4**) and the junction between cingulate and sensory cortex **(A5)**. The same configuration is used for MAP2 **(B)**, Neurofilament **(C)**, and GFAP **(D)** to characterize the pathology of the dendrite, axons, and astrocytes.

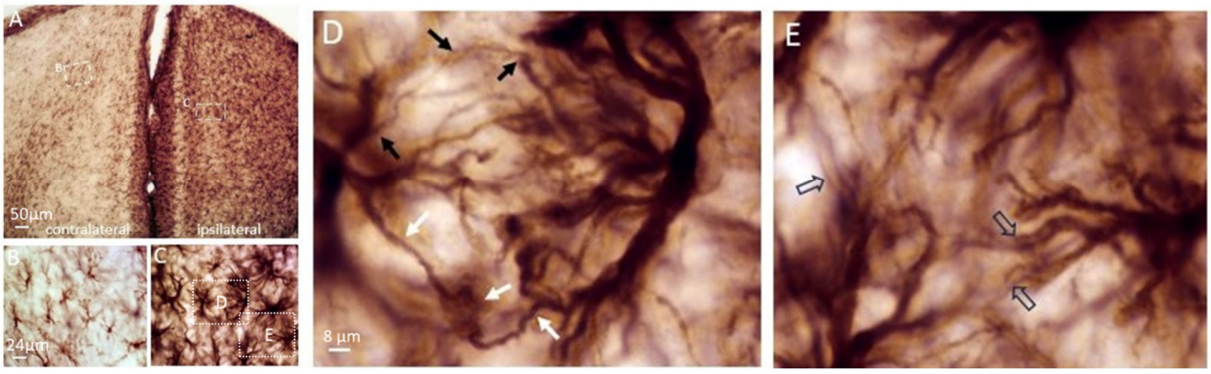

Fig. S7. Acute astrocytic activation in a neonatal mouse brain at 3 hrs after HI-injury. (A-C) GFAP staining shows prominent astrocyte activation in the ipsilateral cingulate compared to the contralateral cingulate cortex (same as **Fig. 5H**). **(D-E)** Zoomed-in views of **(C)** that shows apparent swelling in the astrocytic processes, as indicated by the arrows.

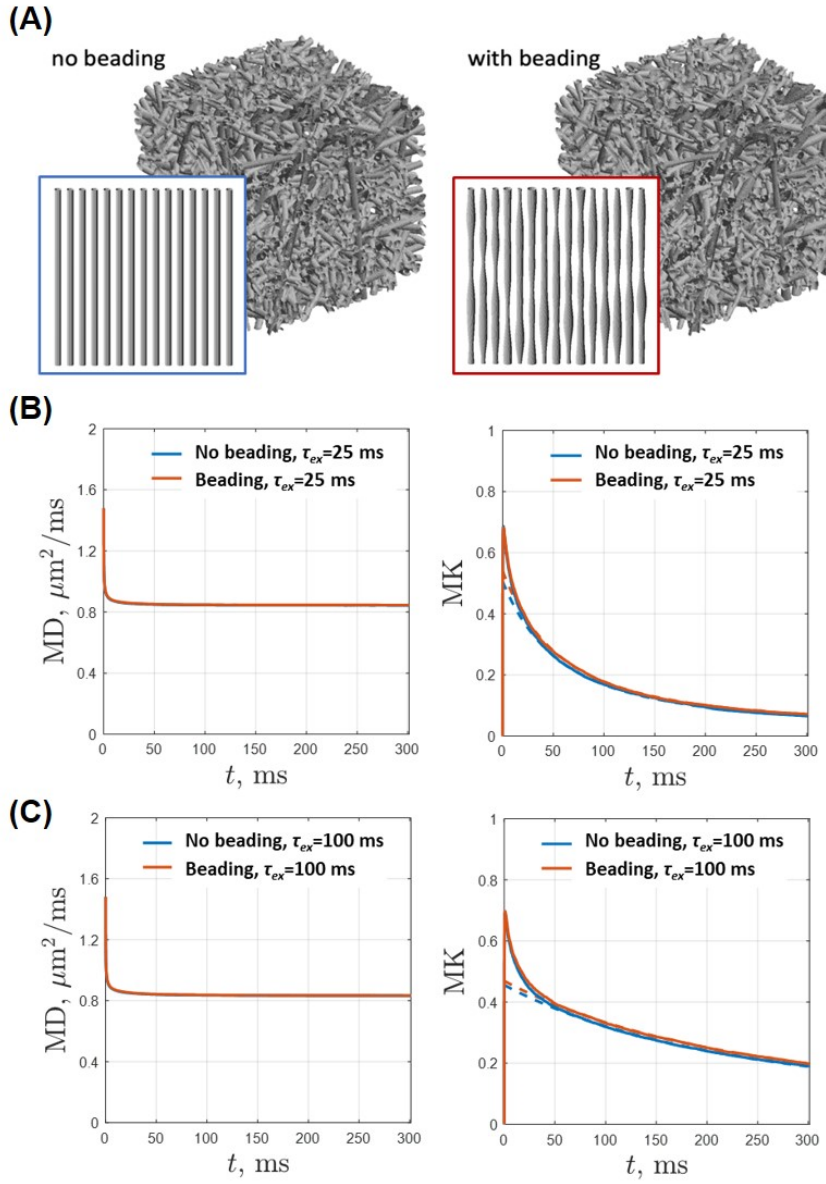

Fig. S8. Diffusion simulations in two substrates composed of randomly positioned, randomly oriented fibers with and without beadings. (A) Illustration of neurite phantoms with and without beading. The simulated *t*-dependent mean diffusivity (MD) and mean kurtosis (MK) in the two substrates with preset τ_{ex}s of 25 ms **(B)** and 100ms **(C)**. The MD and MK curves with and without beading are almost identical, indicating the diffusion coarse-graining over the beading structure has a negligible effect on *t*-dependence. Dashed curves indicate Kärger model fitting results.

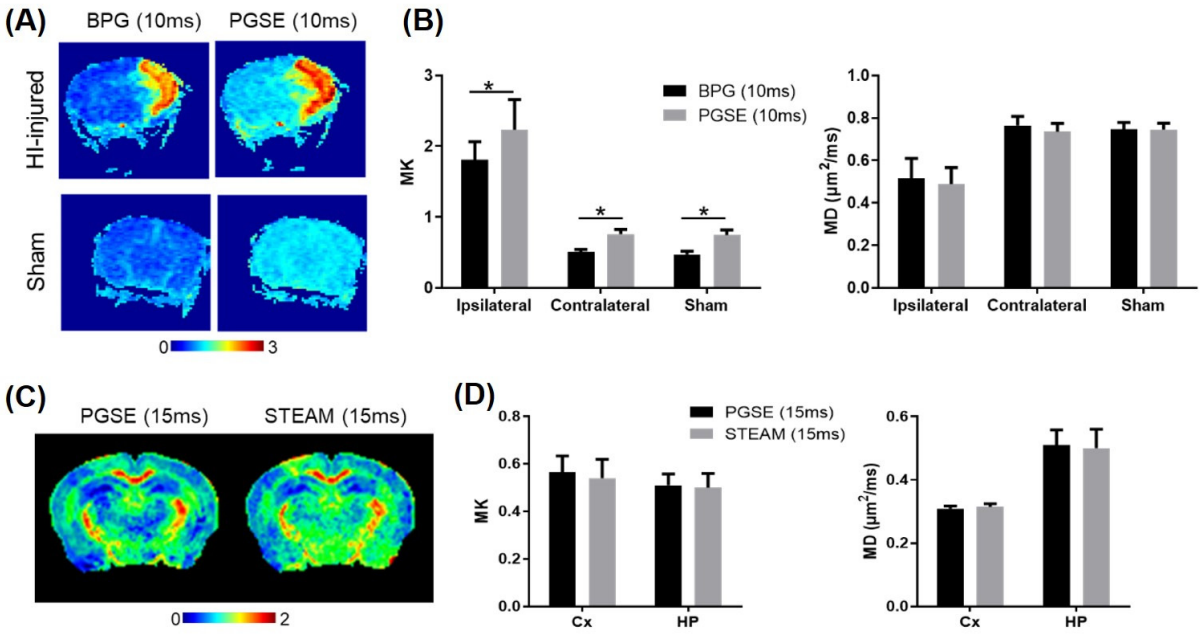

Fig. S9. Comparisons of different diffusion MRI encoding schemes. (A) BGP and PGSE based kurtosis maps with a *t* of 10 ms from HI-injured and sham mice. **(B)** Statistical comparison showed significantly lower ($p<0.05$, $n=6$) MK values obtained using the BGP sequence than those obtained using the PGSE sequence, while the MD values obtained using the two sequences were comparable in both injured and sham mice. **(C)** PGSE and STEAM based kurtosis maps with a *t* of 15 ms from a normal mouse brain. **(D)** Statistical comparison showed no difference ($p>0.05$, $n=5$) in MK or MD values between the two sequences.

Table S1. Root Mean Square Error (RMSE) of the estimated τ_{ex} at different baseline settings and different SNRs.

RMSE of τ_{ex} [ms] for the cylinder phantoms					
SNR / τ_{ex} [ms]	**20**	**30**	**50**	**100**	**INF**
10	7.95	3.28	2.00	1.00	0.81
20	3.98	3.00	1.64	0.83	0.42
30	4.41	2.56	1.29	0.67	0.36
40	3.90	1.89	0.78	0.28	0.14
50	2.61	0.91	1.01	1.35	1.52
75	3.65	1.60	0.57	0.22	0.25
100	4.70	2.51	1.37	0.87	0.68
RMSE of τ_{ex} [ms] for the sphere phantoms					
SNR / τ_{ex} [ms]	**20**	**30**	**50**	**100**	**INF**
10	26.30	14.41	8.75	7.24	7.74
20	7.91	5.29	5.14	5.67	6.19
30	4.13	4.46	5.34	5.87	6.20
40	6.18	7.83	8.82	9.29	9.53
50	7.37	8.98	9.86	10.26	10.44
75	14.98	16.37	17.05	17.30	17.34
100	25.63	26.65	27.07	27.15	27.03

Table S2. Summary of the *in vivo* mouse brain experiment of neonatal HI injury. The numbers of mice that had complete *t*DKI scans at 3 hrs and 48 hrs after HI for each group. Note that, among the 41 mice used in this study, not all mice had complete good-quality *t*DKI scans due to insufficient scan time, animal death, image quality issues, etc.

	Severe injury	**Mild/moderate**	**Sham**
3hr MRI	12	10	6
48hr MRI	8 (follow-up)	6 (follow-up)	5

Table S3. Statistical analysis associated with Fig. 4C. Differences in mean diffusivity (MD) and mean kurtosis (MK) between the ipsilateral and contralateral hippocampus of the severely HIE mice (n=12), as well as the sham mice (n=6), at 3 hrs after HI injury. The comparisons were performed for *t* from 4-10 ms using the bipolar pulsed gradient (BPG) and from 7-40 ms using the pulse gradient spin-echo (PGSE) sequence. The differences between each pair of comparison were shown. * $p<0.05$, ** $p<0.01$, and *** $p<0.001$ by t-test.

	MD			MK		
	Ipsi - Contra	Ipsi - Sham	Contra - Sham	Ipsi - Contra	Ipsi - Sham	Contra - Sham
BPG 4 ms	-0.046**	-0.020	0.025	0.136***	0.092***	-0.044
BPG 5 ms	-0.049**	-0.026	0.023	0.145***	0.111***	-0.033
BPG 6 ms	-0.044**	-0.036*	0.008	0.152***	0.088***	-0.065*
BPG 7 ms	-0.053***	-0.026	0.027	0.125***	0.106***	-0.019
BPG 8 ms	-0.048***	-0.027	0.021	0.147**	0.108**	-0.039
BPG 10 ms	-0.059***	-0.037**	0.022	0.076	0.070	-0.006
PGSE 7 ms	-0.034	-0.005	0.029	0.137*	0.101	-0.036
PGSE 10 ms	-0.034	-0.018	0.016	0.156**	0.111	-0.045
PGSE 15 ms	-0.044	-0.030	0.014	0.145*	0.120*	-0.025
PGSE 20 ms	-0.061	-0.029	0.032	0.085	0.087	0.002
PGSE 40 ms	-0.056	-0.037	0.019	0.102	0.080	-0.022

Table S4. Statistical analysis associated with Fig. 5C. Comparing MD values in the cingulate and sensory cortex of the HIE mice at 3 hrs (n=12) and 48 hrs (n=8) after HI injury, for t from 4-40ms. The differences between each pair of comparison were shown. * p<0.05, ** p<0.01, and *** p<0.001 by paired t-test.

MD	3 hrs	48 hrs			48hrs – 3hrs	
	Cingulate - Sensory	Cingulate - Sensory	Cingulate – contralateral	Contra - contralateral	Cingulate	Sensory
BPG 4 ms	0.0296	0.2505***	0.0339	-0.2166***	-0.1608***	0.0601
BPG 5 ms	0.0460	0.2407***	0.0326	-0.2081***	-0.1689***	0.0258
BPG 6 ms	0.0634	0.2554***	0.0289	-0.2265***	-0.1787***	0.0133
BPG 7 ms	0.0600	0.2526***	0.0334	-0.2192***	-0.1809***	0.0118***
BPG 8 ms	0.0628	0.2620***	0.0344	-0.2276***	-0.1866***	0.0126
BPG 10 ms	0.0651	0.2688***	0.0385	-0.2304***	-0.2047***	-0.0010
PGSE 7 ms	0.0432	0.2544***	-0.005	-0.2595***	-0.1524**	0.0588
PGSE 10 ms	0.0293	0.2697***	0.0114	-0.2583***	-0.1757***	0.0647
PGSE 15 ms	0.0301	0.2807***	0.0291	-0.2516***	-0.1969***	0.0537
PGSE 20 ms	0.0364	0.2785***	0.0305	-0.2480***	-0.2119***	0.0302
PGSE 40 ms	0.0385	0.2789***	0.0261	-0.2528***	-0.2435***	-0.0031

Table S5. Statistical analysis associated with Fig. 5C. Comparing MK values in the cingulate and sensory cortex of the HIE mice at 3 hrs (n=12) and 48 hrs (n=8) after HI injury, for *t* from 4-40ms. The differences between each pair of comparison were showed. * $p<0.05$, ** $p<0.01$, and *** $p<0.001$ by paired t-test.

MK	3 hrs	48 hrs			48hrs – 3hrs	
	Cingulate - sensory	Cingulate - sensory	Cingulate – contralateral	Contra - contralateral	Cingulate	sensory
BPG 4 ms	0.1139	-0.8904***	0.4999**	1.390***	0.3239	-0.6804***
BPG 5 ms	0.1435	-0.9258***	0.5647**	1.490***	0.3935	-0.6757***
BPG 6 ms	0.1213	-0.9200***	0.5815***	1.502***	0.3753	-0.6660***
BPG 7 ms	0.1155	-0.9219***	0.6148***	1.537***	0.4408*	-0.5965***
BPG 8 ms	0.1269	-0.9460***	0.5634**	1.509***	0.4642*	-0.6087***
BPG 10 ms	0.1924	-0.9548***	0.5728**	1.528***	0.4599*	-0.6873***
PGSE 7 ms	0.0602	-1.130***	0.6384***	1.769***	0.2751	-0.9156***
PGSE 10 ms	0.2055	-1.137***	0.7467***	1.884***	0.3259	-1.017***
PGSE 15 ms	0.2459	-1.016***	0.7816***	1.797***	0.3073	-0.9545***
PGSE 20 ms	0.2891	-0.9254***	0.7476***	1.673***	0.3338	-0.8808***
PGSE 40 ms	0.2469	-0.5768**	0.6544***	1.231***	0.3043	-0.5194*

Table S6. Basic demographic and clinical information of the stroke patients who underwent *t*DKI scans.

No.	5
Age, mean (SD), y	70(12)
Sex	
Men	0
Women	5
Medical history	
Hypertension	1
Hyperlipidemia	1
Previous stroke	1
Others (Insomnia)	1
None	1
Baseline clinical characteristics, median (IQR)	
GCS score	13（11-15）
NIHSS score	11.3 (4-19.3)
Systolic blood pressure, mm Hg	157.6 (135.0-186.5)
Glycemia, mmol/Dl	6.4 (5.1-7.6)
Baseline imaging	
Onset-to-imaging time, median (IQR), h	4 (1-22)
Site of occlusion	
L-M1 and R-M1	1
L-M1	1
R-M1	3
Treatment received	
Intravenous thrombolysis alone	1
Intravenous thrombolysis and thrombectomy	1
Thrombectomy alone	0
No reperfusion therapy	3

Table S7. Statistical analysis associated with Fig. 6D. Comparing K_0 and τ_{ex}^* values in the lesions and contralateral uninjured regions of five stroke patients. The differences between the comparisons were showed. * $p<0.05$, ** $p<0.01$ by t-test.

	K_0			τ_{ex}^* [ms]		
	injured region	uninjured region	p value	injured region	uninjured region	p value
Patient 1	0.9139	0.7786	0.0087**	94.75	122.90	0.0411*
Patient 2	0.8426	0.6313		56.78	116.93	
Patient 3	0.7362	0.5424		176.98	230.47	
Patient 4	0.7482	0.5811		112.14	156.24	
Patient 5	0.9798	0.5151		85.96	121.17	

Table S8. The effective b-value in the b0 image (no diffusion-encoding) at different *t*'s in the DW-STEAM sequence.

diffusion time [ms]	50	100	150	200	250
effective b value [ms/μm^2]	8.1	19.8	31.5	43.1	54.8